Journal of Applied Polymer Science

Influence of a rigid polystyrene block on the free volume and ionic conductivity of a gel polymer electrolyte based on poly(methyl methacrylate)-*block*-polystyrene

Xinghua Guan,[1,2] Fang Chen,[1,2] Zhiguang Li,[1,2] Hualong Zhou,[1,2] Xiaoyan Ma[1,2]

[1]Key Laboratory of Space Applied Physics and Chemistry, Ministry of Education, Shaanxi Province, School of Science, Northwestern Polytechnical University, Xi'an 710129, China

[2]Key Laboratory of Polymer Science and Technology, Shaanxi Province, School of Science, Northwestern Polytechnical University, Xi'an 710129, China

Correspondence to: X. Ma (E-mail: m_xiao_yana@nwpu.edu.cn)

ABSTRACT: Diblock copolymers poly(methyl methacrylate)-*block*-polystyrene with three different molar ratios [poly(methyl methacrylate)/polystyrene (PS) = 1:1, 1:1.5, and 1:1.8] were synthesized by atom transfer radical polymerization and used as a polymer matrix for gel polymer electrolytes (GPEs). The positron annihilation lifetime spectroscopy was applied to determine the free-volume behaviors of different GPEs, respectively. We illustrated that a proper PS ratio may led to the formation of a high fraction of free volume, and the influence of the PS ratio on the free-volume fraction was caused by the different morphologies of the GPEs because of the different packing densities of the PS rigid block. The ionic conductivity was correlated with the free volume in the GPE through the study of the ionic conductivity dependence on the temperature; this followed the Vogel–Tamman–Fulcher equation. Moreover, an ionic conductive model was proposed, in which variations of the free-volume behavior provide different ionic-conducting abilities. Thermogravimetric analysis indicated that GPEs based on different block copolymers exhibited high liquid-electrolyte preservation properties. © 2016 Wiley Periodicals, Inc. J. Appl. Polym. Sci. **2016**, *133*, 43901.

KEYWORDS: gels; ionic liquids; polystyrene

Received 21 November 2015; accepted 1 May 2016
DOI: 10.1002/app.43901

INTRODUCTION

Lithium-ion batteries have become the leading portable power source, particularly for consuming electronics devices, because of their advantages of high power density, long recycling life, and high specific capacity.[1–4] Recently, many researchers have expected to apply lithium-ion batteries, with their higher power density, to the development of electrical vehicles with extended long distances.[5–9] Conventional liquid electrolytes exhibit rapid and high ion conductivity when they are treated as principle electrolyte materials in current lithium-ion batteries. However, technical obstacles to the commercial viability of liquid-electrolyte lithium-ion batteries are mainly attributed to the poor stability and flammability, which are due to the leakage or evaporation of the organic solvent. Gel polymer electrolytes (GPEs) containing lithium ions present a high ionic conductivity and excellent compatibility with electrodes during the charge–discharge cycling processes through the immersion of liquid electrolyte in a continuous polymer matrix.[5–8,10] Many types of matrix polymers can be used to prepare GPEs. These polymers include poly(ethylene oxide),[9,11–14] polyacrylonitrile,[11] poly (methyl methacrylate) (PMMA),[15–18] poly(vinyl chloride),[19] and poly(vinylidene fluoride).[20,21]

PMMA has become one of the most commonly used polymer matrixes in GPEs because of their high ion solvation and transportation ability, which are due to the polarity and excellent compatibility with electrodes. PMMA-based gel electrolytes have a high ionic conductivity and good electrochemical stability. However, pure PMMA cannot meet current demands because of its low mechanical strength; this results in the restriction of applications of PMMA-based GPEs. The mechanical strength increases significantly with the increasing percentage of PMMA.[22] Indeed, the use of copolymers as polymer matrixes in GPEs is a quite promising approach because of the combination of the advantages of different segments, such as comblike copolymers.[23] In our previous studies, we found that comblike PMMA-based copolymers with rigid segments in the main

Additional Supporting Information may be found in the online version of this article.

chain and soft segments as branches are promising polymer matrixes for GPEs.[24–26] This will lead to a larger liquid-electrolyte absorption of GPEs and will enhance the ionization of lithium perchlorate ($LiClO_4$) and improve the migration of Li^+. Meanwhile, block copolymers (BCPs) have been investigated as functional polymers matrixes for GPEs because the ability to tune the ionic conductivity and mechanical strength through immersion advantages of two different blocks via covalent bonds.[20,27–29] In general, the structure of the rigid block can give the gel system higher mechanical properties and thermal stability, whereas the soft polar block can offer the gel system a favorable ionic conductivity because of outstanding compatibility with the liquid electrolyte.[30] In addition, the self-assembly behavior of the microphase separation of BCPs may form a continuous ionic path, and this can contribute to ionic conductivity.[31–33]

However, until now, the dependence of the free volume on the ionic conductivity caused by compositional factors of BCPs has rarely been reported. It will be a promising achievement if the relationship between the free volume and ionic conductivity of BCP-based GPEs are clearly studied.

We chose positron annihilation lifetime spectroscopy (PALS) as the approach to study the free-volume behavior of GPEs; this is the technique used to determine the free-volume behavior in solid materials such as polymers through the probing of the lifetime of *ortho*-positronium (*o*-Ps). The PALS technique has been applied to many polymeric systems, including polymer-in-salt electrolytes[34] and proton-exchange membrane fuel cells,[35,36] for free-volume behavior determination. It has almost been agreed that a correlation exists between the free volume and the ionic conductivity.[34,37–40] PALS will provide enough free-volume characters of different GPEs based on different poly(methyl methacrylate)-*block*-polystyrene (PMMA-*b*-PS block) copolymers. Polystyrene (PS) has exhibited good mechanical performances. As a result, the PMMA-*b*-PS BCP can improve the mechanical stability of the gel electrolytes.

For this purpose, we used PMMA-*b*-PS BCPs with different PS chain lengths as model polymer matrixes, preparing GPEs by immersing them with liquid electrolyte. The aim of this study was to investigate the influence of the PS ratio on the GPE free volume and its correlation between the segmental mobility and ionic conductivity.

EXPERIMENTAL

Materials

Styrene and methyl methacrylate were purchased from Tianjin Fuchen Chemical Reagents Factory (China). Methyl methacrylate was washed with a 5% sodium hydroxide solution to remove the inhibitor and then with distilled water until the monomer became neutral. A specific amount of magnesium sulfate was added to the solution after 24 h, and then, the solution was vacuum-distilled at 60 °C. The styrene was treated with the same procedure. However, the final vacuum distillation was applied at 80 °C.

Copper(I) chloride (CuCl) was added to glacial acetic acid and stirred without light for 10 h. The obtained solution was

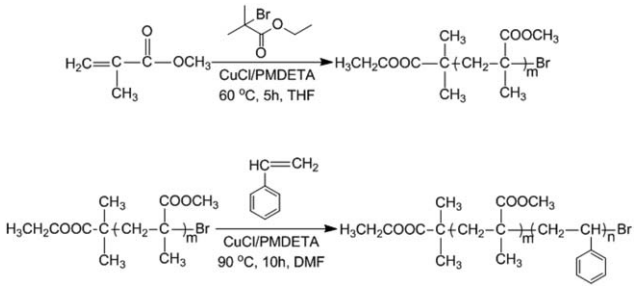

Scheme 1. Synthesis of the PMMA–Br and PMMA-*b*-PS copolymers.

washed with ethanol and then acetone until the color turned gray–white. The prepared CuCl powder was heated for 24 h in a vacuum at 40 °C and then placed in a light-resistant bottle. Tetrahydrofuran (THF) was distilled under atmospheric pressure at 70 °C after reflux with sodium. Dimethylformamide (DMF) was applied after vacuum distillation at 90 °C. Pentamethyldiethylenetriamine (PMDETA) and ethyl 2-bromoisobutyrate were purchased from Aladdin Reagent (China) Co., Ltd., and were used without further purification.

Electrochemical-device-grade propylene carbonate (PC) was dried by 4-Å molecular sieves. $LiClO_4$ was dried at 120 °C for 1 h and dissolved in PC to prepare polymer electrolytes with a concentration of 1 mol/L.

Synthesis of PMMA-*b*-PS

Three PMMA-*b*-PS BCPs with different PMMA and PS ratios were synthesized through two-step atom transfer radical polymerization, as shown in Scheme 1, through the tuning of the feeding ratio of styrene in second step.[41]

To synthesize the macroinitiator, the reactants, including methyl methacrylate, CuCl, PMDETA, and ethyl 2-bromoisobutyrate, with a molar ratio of 100:1:2:1 were added to certain amount of THF (solvent), and they were all placed in a three-necked flask. After the mixture solution was cooled to 0 °C, a vacuum and nitrogen gas were applied the sequential solution with stirring at 60 °C for 5 h under a nitrogen atmosphere. The obtained solution was filtered through an alumina column to remove cupric ion. Then, a white precipitate was obtained through the addition of methanol. The macroinitiator was dried overnight at 40 °C under reduced pressure. The ^{1}H-NMR spectrum of the macroinitiator is shown in Figure S1 in the Supporting Information.

Three PMMA-*b*-PS copolymers with different block ratios were synthesized through changes in the feed amount of styrene with the previously obtained macroinitiator. Three reagent mixture compositions, including styrene, PMMA–Cl, CuCl, and PMDETA with molar ratios of (50, 100, or 150):50:1:2, were mixed in sequence in a three-necked flask with THF as the solvent. After a process of frozen-vacuum releasing three times, the solutions were stirred at 90 °C for 10 h under a nitrogen atmosphere. The obtained solution was filtered through an alumina column for the removal of cupric ion. Then, a white precipitate PMMA-*b*-PS was obtained through the addition of methanol. The ^{1}H-NMR spectra of three BCPs is shown in Figure S2 in the Supporting Information.

Table I. Free-Volume Parameters of the Four GPE Membranes at 25 °C

Sample	PMMA	PMMA-*b*−1PS	PMMA-*b*−1.5PS	PMMA-*b*−1.8PS
τ_3 (ns)	2.22 ± 0.013	2.15 ± 0.012	2.09 ± 0.012	2.08 ± 0.012
I_3 (%)	9.78 ± 0.063	10.97 ± 0.068	10.84 ± 0.072	10.35 ± 0.077
R (Å)	3.04 ± 0.10	2.99 ± 0.14	2.93 ± 0.22	2.92 ± 0.17
V (Å^3)	118.03 ± 0.11	111.41 ± 0.22	105.69 ± 0.54	103.86 ± 0.32
F_r	11.54 ± 0.01	12.22 ± 0.02	11.46 ± 0.04	10.75 ± 0.03

The average molecular weights of the PMMA macroinitiator and BCPs were determined through gel permeation chromatography (GPC) calibrated with standard PS and with THF as the eluent. A Waters 1515 GPC instrument was used at an elution rate of 1 mL/min. The PMMA macroinitiator and three different BCPs were shown with different number-average molecular weights, which were 15,800 (polydispersity index = 1.12), 32,900 (polydispersity index = 1.38), 39,600 (polydispersity index- = 1.21), and 44,400 (polydispersity index = 1.15), respectively.[42] The three different BCPs were named PMMA-*b*-1PS, PMMA-*b*-1.5PS, and PMMA-*b*-1.8PS, respectively, on the basis of the molar ratio, as determined by GPC and ^{1}H-NMR.

Preparation of the GPEs

A liquid electrolyte was prepared by the dissolution of $LiClO_4$ in a plasticizer PC to obtain an $LiClO_4$ solution with a concentration of 1 mol/L. The GPE precursor was prepared by the mixture of the polymer THF solution and liquid electrolyte under sonification, in which the weight ratio of the polymer matrix and liquid electrolyte was 40:60. The solutions obtained were cast on a PTFE plate to enable the solvent to gradually evaporate at 40 °C for approximately 12 h, as we usually did for other GPE systems[24] to obtain the polymer gel electrolytes.

PALS

All PALS measurements were performed with a fast–fast coincidence system at time resolution of 280 ps at room temperature. For each sample, the polymer films were stacked to obtain sample plates approximately 1.5 mm in thickness and 1 cm in diameter. The positron source (20 μCi), Na, was sandwiched between two identical pieces of the samples. Each spectrum contained approximately 1×10^6 and 4×10^6 counts of the positron annihilation technique fitting and maximum third lifetime methods, respectively.

Ionic Conductivity

Impedance spectra were performed with an HIOKI-3532 LRC meter with a frequency range of 42 Hz to 5 MHz and a temperature range of 20 to 50 °C. The GPE with a 1 × 1 cm square and thickness around 100 μm were placed between two stainless steel electrodes, were applied for impedance measurements. The ionic conductivity was calculated with the following equation:

$$\text{Ionic conductivity} = L/(S \times R_b) \quad (1)$$

where R_b is the bulk resistance of the GPE obtained by the impedance spectra, L is the thickness of the GPE membrane (cm) and is equal to 0.10 ± 0.02 mm, and S is the contact area between the electrolyte membrane and stainless steel electrode (cm^2) and is equal to 1 cm^2.

Thermal Analysis of the GPEs

Differential scanning calorimetry analysis of the GPEs was performed with a Mettler DSC1 differential scanning calorimeter at a heating rate of 10 °C/min and in the temperature range of −100 to 150 °C under an N_2 atmosphere.

Thermogravimetric analysis (TGA) was conducted with a TA Q500 thermogravimeter under an N_2 atmosphere at a heating rate of 10 °C/min.

RESULTS AND DISCUSSION

Free-Volume Behavior by PALS

PALS was performed quantitatively on each of the GPE samples to define the free-volume characteristics of the GPEs. The nanohole shape was assumed to be spherical. As described for the PALS measurement on polymer materials by many other researchers, all of the measured spectra were resolved into three components with positron annihilation technique fitting for discrete analysis. The first lifetime component ($\tau_1 = 0.125$ ns) and the intermediate lifetime component ($\tau_2 = 300$–400 ps) were attributed to the self-annihilation of *para*-positronium and positron annihilation, respectively. The third lifetime component ($\tau_3 > 1$ ns) resulted from the pickoff annihilation of *o*-Ps with different distributions of free-volume holes, which mainly represented the free-volume information of the polymer. The relation between the *o*-Ps lifetime and the radius of the free-volume holes (R) followed the equation[43]:

$$\tau_3 = \frac{1}{2}\left[1 - \frac{R}{R+1.656} + \frac{1}{2\pi}\sin\left(\frac{2\pi R}{R+1.656}\right)\right]^{-1} \quad (2)$$

On the basis of the free-volume theory proposed by Tao and Eldrup,[44,45] *o*-Ps particles reside in a spherical potential well and possess an infinite potential barrier of radius R_0. The thickness of the electron layer formed on the wall of the hole is presented as ΔR. Subsequently, the effective radius of the layer becomes $R = R_0 - \Delta R$. The fitting of the observed *o*-Ps lifetimes in polymers with known hole sizes indicates that ΔR is 1.656 Å. The average free-volume size (V) is defined as follows:

$$V = \frac{4\pi R^3}{3} \quad (3)$$

The relative intensity of the longest living component (I_3) is correlated with the intensity of the free-volume hole. The fraction of the free volume (F_r) is evaluated with eq. (4):

$$F_r = VI_3 \quad (4)$$

The free-volume-related parameters were calculated from eqs. (2)–(4) and are listed in Table I.

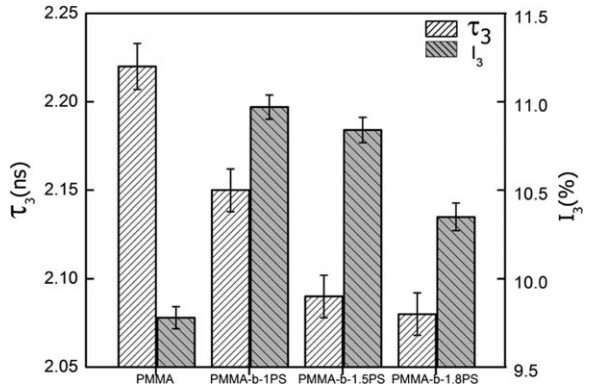

Figure 1. Lifetimes (τ_3 and I_3 values) for the four GPE systems with different PS ratios.

We picked τ_3 and I_3 of four different GPE systems and drew a bar graph to illustrate the free-volume change as the PS block ratio increased, as shown in Figure 1. After comparing the parameters of the four GPE systems, we observed that τ_3 of the pure PMMA-based GPE (2.22 ns) decreased with increasing PS ratio in the copolymer matrix. I_3 and F_r reached the highest values for the PMMA-*b*-1PS based GPE and decreased at a higher PS ratio. The higher τ_3 was detected for the pure PMMA-based GPE because of the amorphous phase with a random configuration of polymer chains. With the introduction of the PS block, the formation of the ordered phase caused a reduction in τ_3 because there was more PS block in a denser and packed state. A comparison of the average free-volume hole diameters of different GPEs suggested free-volume holes of similar sizes for all of the GPEs. However, the total fraction of the free volume (I_3 and F_r) increased significantly for PMMA-*b*-1PS because of the high packing density of the rigid PS region under a proper PS ratio. When the proper PS ratio was exceeded, a decrease in the free volume was detected because of the irregular packing pattern of the PS region.

The continuous analyses of the *o*-Ps lifetime distribution by the programming of the maximum entropy lifetime method of different GPEs at 25 °C are shown in Figure 2. The border distribution was obtained for the GPE of pure PMMA. With the introduction of the PS rigid block, the *o*-Ps lifetime distribution turned into a two-peak distribution for the GPE with PMMA-*b*-1PS. Beyond this PS block ratio, it turned back into a single distribution. This phenomenon illustrated that the rigid PS block ratio may have had different influences on the *o*-Ps lifetime distribution because of the packing density of the ordered PS region in the GPE. With a proper ratio of PS (PMMA-*b*-1PS), which could cause an increase in the ordered region by enhancing the packing density of the PS domain, two different *o*-Ps lifetime distribution were observed.[46] A similar tendency of two *o*-Ps lifetimes was reported to be due to different phase states of the polymer.[36] The free-volume fraction depended on the ordered or amorphous phase of the polymer, in which the larger free volume was attributed the amorphous domain, as shown by the long *o*-Ps lifetime and vice versa. This may give us a clue that phase separation could have occurred in PMMA-*b*-1PS because of the enhancement of the packing density of PS. When the proper PS ratio was exceeded, the inhibition of the formation of the rigid PS domain was introduced because of the poor PS packing pattern with longer PS blocks.

Ionic Conductivity and Dependence on Temperature

To investigate the influence of the PS block ratio on the ionic conductive behavior, we used electrochemical impedance spectroscopy (EIS) spectroscopy of the four GPEs at different temperatures, as shown in Figure 3. The shapes of the EIS curves were different with the introduction of the PS block, and this was mainly attributed to the electrode/electrolyte behavior difference. For the GPE based on pure PMMA, the EIS spectra showed that a semicircle at higher frequencies corresponded to the charge transfer limited process and the linear portion at lower frequencies corresponded to the diffusion process. It was reasonable that the charge transfer resistance decreased with increasing temperature for the GPE based on PMMA. All of the GPEs based on different PS block ratios showed the disappearance of the semicircle at higher frequencies because of the faster charge transfer caused by the enhancement of the electrode/electrolyte interfacial behavior.

To understand the ionic conductivity behavior among the GPEs with different PS block ratios, the impedance differences from 20 to 50 °C are shown in Figure 4. Including the pure PMMA GPE, the four GPEs showed similar tendencies of impedance, which decreased with increasing temperature.

The dependence of the conductivity on temperature was determined in the temperature range from 20 to 50 °C. The impedance plots of the membranes at different temperatures are shown in Figure 4, which shows a significant increase in the ionic conductivity in the range of all of the GPE systems from 20 to 50 °C. All of the GPEs of the copolymer showed a higher conductivity than that of the pure PMMA. PMMA-*b*-1PS exhibited the highest ionic conductivity among the four GPEs.

As all we know, the ionic conductivity depends on the mobility of the polymer segment and on the size and density of the free-volume cavity.[24,28,29] The polymer segmental mobility was enhanced with increasing temperature; this benefitted ion-hopping among

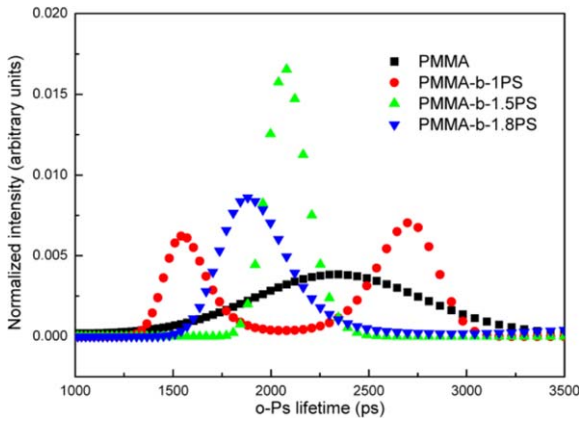

Figure 2. *o*-Ps lifetime distributions for the four GPE membranes. [Color figure can be viewed in the online issue, which is available at wileyonlinelibrary.com.]

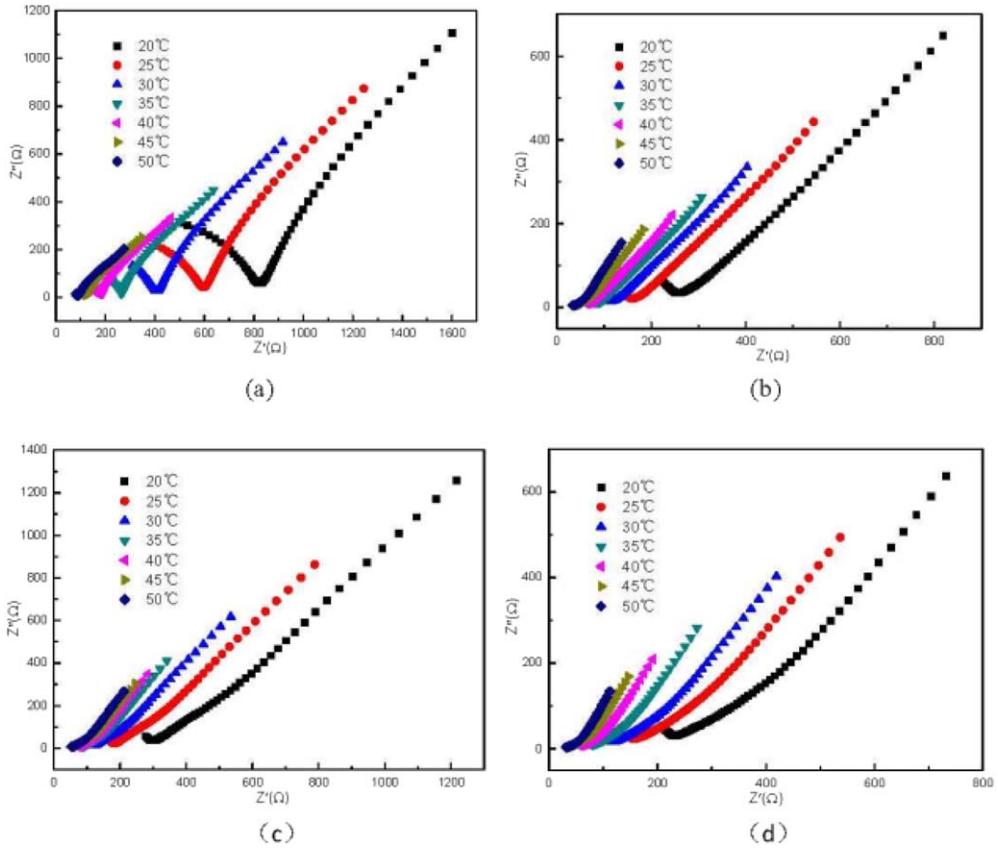

Figure 3. EIS spectra of GPEs based on (a) 40 wt % PMMA, (b) 40 wt % PMMA-*b*−1PS, (c) 40 wt % PMMA-*b*-1.5PS, and (d) 40 wt % PMMA-*b*−1.8PS at different temperatures. Z′ = the real part of the impendence; Z″ = the imaginary part of the impendence. [Color figure can be viewed in the online issue, which is available at wileyonlinelibrary.com.]

polymer backbone. Meanwhile, an increase in the free volume led to an increase in the mobility of both the ion and segmental mobility, and this all favored ion transportation. Thus, the ions could be transported through the free volume, and this raised the conductivity of the GPE system.[20,47] We found that both a higher free volume and a higher ionic conductivity in the GPE-based PMMA-*b*-1PS.

To better investigate the ionic conductive mechanism, the conductivity–temperature relationship was fitted with the Vogel–Tamman–Fulcher (VTF) empirical equation. In our system, it was reasonable for the measured glass-transition temperature of the soft PMMA block (T_{g2}) to be used as a reference temperature (T_0) to fit the VTF equation, which is shown to have excellent fitting in Figure 5:

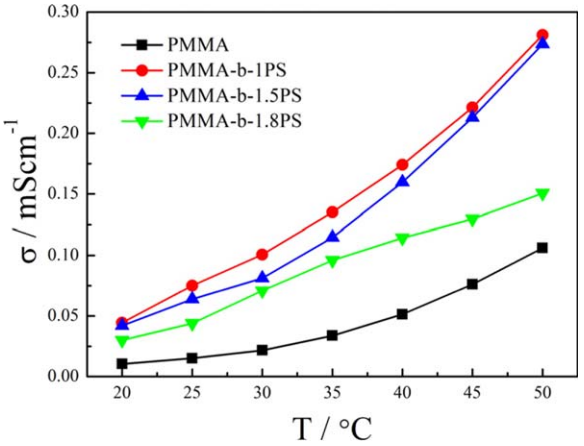

Figure 4. Dependence of the ionic conductivity (σ) on the temperature (T) for the four GPEs. [Color figure can be viewed in the online issue, which is available at wileyonlinelibrary.com.]

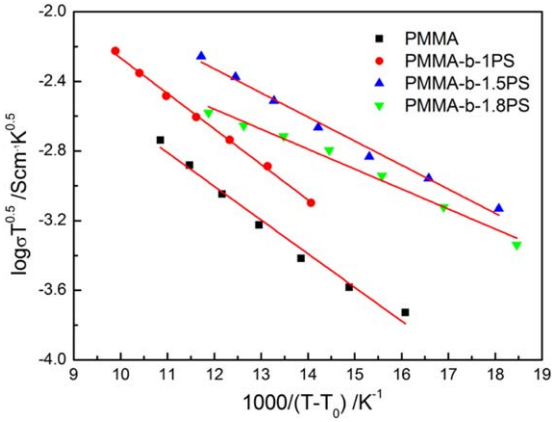

Figure 5. VTF plots for the four GPEs. σ = ionic conductivity; T = temperature; T_0 = reference temperature. [Color figure can be viewed in the online issue, which is available at wileyonlinelibrary.com.]

Table II. Fitting Parameters of the VTF Equation: *A* and *E*

Sample	PMMA	PMMA-*b*-1PS	PMMA-*b*-1.5PS	PMMA-*b*-1.8PS
T_g (°C)	7.81	−1.11	14.69	15.83
A (S cm^{-1} K$^{-1/2}$)	0.21	0.59	0.22	0.07
E (meV)	4.0	4.1	3.9	3.7

T_g, glass-transition temperature.

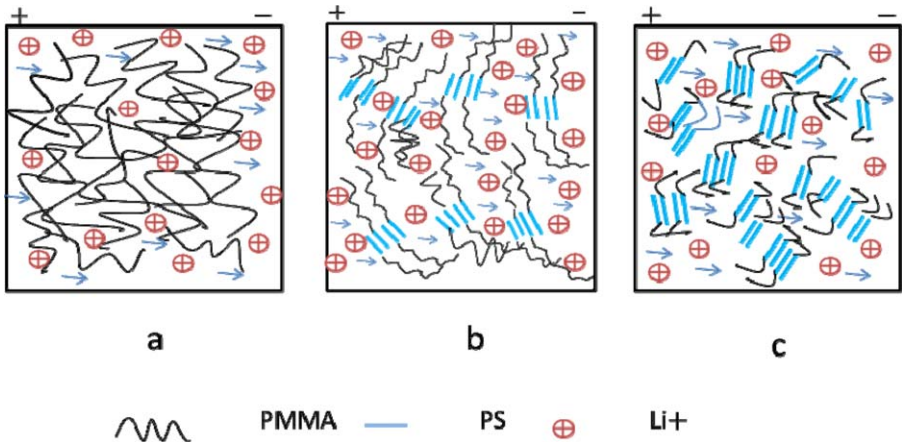

Figure 6. Scheme of the transportation of Li^+ of the GPEs based on the (a) pure PMMA matrix, (b) PMMA-*b*-PS with a longer PS block ratio, and (c) PMMA-*b*-PS with a shorter PS block ratio. [Color figure can be viewed in the online issue, which is available at wileyonlinelibrary.com.]

$$\text{Ionic conductivity} = AT^{1/2}\exp[-E(T-T_0)] \quad (5)$$

where *A* is the pre-exponential factor, *E* is the pseudo-activation energy for the redistribution of the free volume, and *T* is the temperature. The T_{g2} values of the different BCPs were obtained by differential scanning calorimetry (Figure S3, Supporting Information). The *A* and *E* values obtained by the fitting of conductivity data to eq. (5) are given in Table II. The excellent fitting of the VTF equation usually indicates ionic transportation followed amorphous polymer electrolyte behavior.[48] In general, *A* is proportional to the numbers of ionic charge carriers in the electrolyte. We found that PS block ratio was correlated with the density of the charge carrier because it showed a tendency to increase *A* and then decrease with increasing PS ratio. The phenomenon corresponded well with the previous discussion; the number of charge carriers increased with the proper PS block through the formation of a larger free volume. Once that limit was exceeded (1:1 in this system), the numbers of charge carrier decrease with increasing PS ratio because of the reduction in the free volume. The resistance measurement also showed that the enhancement of the charge transfer between the electrode and GPE resulted from the introduction of PS, as discussed previously. The *E* values maintained a value around 4 meV; this showed that the PS block ratio almost did not affect the energy character.

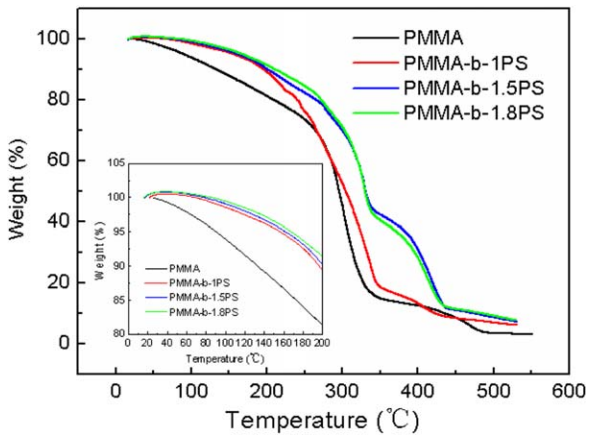

Figure 7. TGA curves of the four GPE membranes. [Color figure can be viewed in the online issue, which is available at wileyonlinelibrary.com.]

Microstructure Morphology Model for the PMMA-*b*-PS Based GPE

On the basis of the previous analysis, we deduced that the microstructure of the GPE, which was related to the free-volume structure, played an important role in determining the ionic conductivity. The reasonable microstructure model for the PMMA-*b*-PS based GPE with different PS ratios is illustrated in Figure 6. For the pure PMMA-based GPE, an amorphous structure with a small free-volume fraction represented a longer *o*-Ps lifetime. The inner chain interactions tended to enhance the entanglement of PMMA segments and cause a decrease in the free-volume fraction in the GPE system; this hindered the transportation of Li^+ and resulted in the lowest ionic conductivity among the GPEs. The introduction of a small amount of PS segments in PMMA-*b*-1PS led to an enhancement in the compatibility of two blocks by

weakening the entanglements of the PMMA chains in GPE and producing a rigid PS microphase. This resulted in an increase in the free-volume fraction. However, with the continuous increase in the PS segmental ratio in the BCP, the free-volume fraction and ionic conductivity of the GPE decreased in comparison with the PMMA-*b*-1PS copolymer-based GPE because the steric hindrance of PS may have caused a larger domain of the PS microphase. This showed us a clear mechanism of the ionic conductivity difference due to the influence of the PS ratio in the BCP.

Liquid-Electrolyte Preservation Property of the GPE Systems

TGA was used to evaluate the preservation of the liquid electrolyte of the GPEs for further battery applications. Figure 7 shows typical TGA curves in the four GPE membranes. Two-step degradation was observed for all of the samples. The first degradation step, from 80 to 340 °C, was attributed to the loss of the PC solvent, whose boiling point was 242 °C. The second degradation step, from 340 to 500 °C, was caused by the decomposition of the polymer matrix. When the weight loss was 5%, the thermal decomposition temperatures of PMMA, PMMA-*b*-1PS, PMMA-*b*-1.5PS, and PMMA-*b*-1.8PS were 90.5, 156.5, 162.0, and 167.9 °C, respectively. These results demonstrate that the introduction of the PS block with different ratios in PMMA obviously improved the thermal stability of the PMMA-based GPEs. Furthermore, the inset in Figure 7 shows the weight loss below 200 °C; it demonstrates the liquid-electrolyte preservation properties of the different GPEs. It shows that a half PC loss was reduced for all of the GPEs containing PMMA-*b*-PS compared to that of the GPE with pure PMMA. It clearly indicates that the PC preservation properties were enhanced through the introduction of the PS block to the PMMA matrix.

CONCLUSIONS

Three BCPs PMMA-*b*-PSs with different block ratios (1:1, 1:1.5, and 1:1.8) were synthesized and evaluated as polymer matrixes for GPEs of lithium-ion batteries. After we compared the PALs data, we found that the PS rigid block length had a great influence on the free-volume behavior of the GPEs. The PMMA-*b*-1PS showed a larger free-volume fraction compared to the pure PMMA and other GPEs with longer PS ratios. The difference in the free-volume behavior was mainly caused by the different packing densities of the PS rigid block, and the ionic conductivity was correlated with the free volume in the study of the ionic conductivity dependence on the temperature; this followed the VTF equation. The results of this study suggest that different rigid PS block lengths may play different roles in segmental packing and this may influence the micromorphology of GPEs and provide different ionic conducting abilities. TGA of the GPE membranes indicated that the introduction of PS significantly enhanced the liquid-electrolyte preservation properties of the GPEs.

ACKNOWLEDGMENTS

The authors are grateful for the support of the Project of the National Natural Science Foundation of China (contract grant number 51103117), the National Natural Science Foundation of Shaanxi Province (contract grant numbers 2013JQ2010 and 2013JM2012), the Northwestern Polytechnical University (NPU) Fundamental Research Foundation (contract grant numbers JC201158 and 3102014JCQ01089), and the Graduate Starting Seed Fund of NPU (contract grant number Z2011015).

REFERENCES

1. Zhang, H. P.; Zhang, P.; Li, Z. H.; Sun, M.; Wu, Y. P.; Wu, H. Q. *Electrochem. Commun.* **2007**, *9*, 1700.
2. Kang, B.; Ceder, G. *Nature* **2009**, *458*, 190.
3. Patil, A.; Patil, V.; Shin, D. W.; Choi, J. W.; Paik, D. S.; Yoon, S. J. *Mater. Res. Bull* **2008**, *43*, 1913.
4. Hassoun, J.; Kim, J.; Lee, D. J.; Jung, H. G.; Lee, S. M.; Sun, Y. K.; Scrosati, B. *J. Power Sources* **2012**, *202*, 308.
5. Rao, M. M.; Geng, X. Y.; Liao, Y. H.; Hu, S. J.; Li, W. *S. J. Membr. Sci.* **2012**, *399*, 37.
6. Wu, N.; Cao, Q.; Wang, X. Y.; Li, X. Y.; Deng, H. Y. *J. Power Sources* **2011**, *196*, 8638.
7. Ryou, M. H.; Lee, Y. M.; Cho, K. Y.; Han, G. B.; Lee, J. N.; Lee, D. J.; Choi, J. W.; Park, J. K. *Electrochim. Acta* **2012**, *60*, 23.
8. Raghavan, P.; Manuel, J.; Zhao, X.; Kim, D. S.; Ahn, J. H.; Nah, C. *J. Power Sources* **2011**, *196*, 6742.
9. Yu, X. Y.; Xiao, M.; Wang, S. J.; Zhao, Q. Q.; Meng, Y. Z. *J. Appl. Polym. Sci.* **2010**, *115*, 2718.
10. Miranda, D. F.; Versek, C.; Tuominen, M. T.; Russell, T. P.; Watkins, J. J. *Macromolecules* **2013**, *46*, 9313.
11. Dissanayake, M. A. K. L.; Bandara, L. R. A. K.; Bokalawala, R. S. P.; Jayathilaka, P. A. R. D.; Ileperuma, O. A.; Somasundaram, S. *Mater. Res. Bull* **2002**, *37*, 867.
12. Rolland, J.; Brassinne, J.; Bourgeois, J. P.; Poggi, E.; Vlad, A.; Gohy, J. F. *J. Mater. Chem. A* **2014**, *2*, 11839.
13. Wang, S.-H.; Hou, S.-S.; Kuo, P.-L.; Teng, H. *ACS Appl. Mater. Interfaces* **2013**, *5*, 8477.
14. Gu, Y.; Zhang, S.; Martinetti, L.; Lee, K. H.; McIntosh, L. D.; Frisbie, C. D.; Lodge, T. P. *J. Am. Chem. Soc.* **2013**, *135*, 9652.
15. Chen, F.; Ma, X.; Qu, X.; Yan, H. *J. Appl. Polym. Sci.* **2009**, *114*, 2632.
16. Ostrovskii, D.; Torell, L. M.; Appetecchi, G. B.; Scrosati, B. *Solid State Ionics* **1998**, *106*, 19.
17. Sharma, R.; Sil, A.; Ray, S. *Polym. Compos.*, to appear. **2016**, *37*, 1936.
18. Luo, D.; Li, P.; Li, Y.; Yang, M. *J. Appl. Polym. Sci.* **2010**, *118*, 1527.
19. Rajendran, S.; Sivakumar, P. *Phys. B* **2008**, *403*, 509.
20. Xiao, Q. Z.; Wang, X. Z.; Li, W.; Li, Z. H.; Zhang, T. J.; Zhang, H. L. *J. Membr. Sci.* **2009**, *334*, 117.
21. Prasanth, R.; Shubha, N.; Hng, H. H.; Srinivasan, M. *J. Power Sources* **2014**, *245*, 283.
22. Xu, J. J.; Ye, H. *Electrochem. Commun.* **2005**, *7*, 829.
23. Liang, Y. H.; Cheng-Chien, W. B.; Chen, C. Y. *J. Power Sources* **2008**, *176*, 340.

24. Wang, Y. F.; Ma, X. Y.; Zhang, Q. L.; Tian, N. *J. Membr. Sci.* **2010**, *349*, 279.
25. Wang, S. H.; Yan, H. X.; Ma, X. Y.; Huang, Y.; Zhang, Q. L. *Acta Polym. Sin.* **2008**, *9*, 880.
26. Wang, S. H.; Yan, H. X.; Ma, X. Y.; Huang, Y. *Acta Polym. Sin.* **2008**, *5*, 442.
27. Darling, S. B. *Prog. Polym. Sci.* **2007**, *32*, 1152.
28. Poree, D. E.; Giles, M. D.; Lawson, L. B.; He, J. B.; Grayson, S. M. *Biomacromolecules* **2011**, *12*, 898.
29. Kriksin, Y. A.; Khalatur, P. G.; Neratova, I. V.; Khokhlov, A. R.; Tsarkova, L. A. *J. Phys. Chem. C* **2011**, *115*, 25185.
30. Young, W. S.; Kuan, W. F.; Epps, T. H. *J. Polym. Sci. Part B: Polym. Phys.* **2014**, *52*, 1.
31. Khandpur, A. K.; Foerster, S.; Bates, F. S.; Hamley, I. W.; Ryan, A. J.; Bras, W.; Almdal, K.; Mortensen, K. *Macromolecules* **1995**, *28*, 8796.
32. Chintapalli, M.; Chen, X. C.; Thelen, J. L.; Teran, A. A.; Wang, X.; Garetz, B. A.; Balsara, N. P. *Macromolecules* **2014**, *47*, 5424.
33. Young, N. P.; Devaux, D.; Khurana, R.; Coates, G. W.; Balsara, N. P. *Solid State Ionics* **2014**, *263*, 87.
34. Forsyth, M.; Sun, J. Z.; MacFarlane, D. R.; Hill, A. J. *J. Polym. Sci. Part B: Polym. Phys.* **2000**, *38*, 341.
35. Lei, M.; Wang, Y. J.; Liang, C.; Huang, K.; Ye, C. X.; Wang, W. J.; Jin, S. F.; Zhang, R.; Fan, D. Y.; Yang, H. J.; Wang, Y. G. *J. Power Sources* **2014**, *246*, 762.
36. Sawada, S.; Yabuuchi, A.; Maekawa, M.; Kawasuso, A.; Maekawa, Y. *Radiat. Phys. Chem.* **2013**, *87*, 46.
37. Stevens, J. R.; Chung, S. H.; Horoyski, P.; Jeffrey, K. R. *J. Non-Cryst. Solids* **1994**, *172*, 1207.
38. Gong, J.; Gong, Z. L.; Yan, X. L.; Gao, S.; Zhang, Z. L.; Wang, B. *Chin. Phys. B* **2012**, *21*, 107803.
39. Gao, S.; Yan, X. L.; Zhong, J.; Xue, G. B.; Wang, B. *Appl. Phys. Lett.* **2013**, *102*, 173903.
40. Peng, Z. L.; Wang, B.; Li, S. Q.; Wang, S. J. *J. Appl. Phys.* **1995**, *77*, 334.
41. Wang, J. S.; Matyjaszewski, K. *Macromolecules* **1995**, *28*, 7901.
42. Guan, X.; Ma, X.; Zhou, H.; Chen, F.; Li, Z. J. *Thermoplast. Compos. Mater.* **2015**, *14*, 1.
43. Zhu, Y. C.; Wang, B.; Gong, W.; Kong, L. M.; Jia, Q. *M. Macromolecules* **2006**, *39*, 9441.
44. Filipecki, J.; Korzekwa, P.; Filipecka, K.; Hyla, M.; Korzekwa, D.; Golis, E.; Korzekwa, W. *Chem. Met. Alloys* **2011**, *4*, 13.
45. Eldrup, M.; Lightbody, D.; Sherwood, J. N. *Chem. Phys* **1981**, *63*, 51.
46. Zhou, W.; Wang, J. J.; Gong, Z. L.; Gong, J.; Qi, N.; Wang, B. *Appl. Phys. Lett.* **2009**, *94*, 021904.
47. Orofino, A. B.; Camezzana, M. F.; Galante, M. J.; Oyanguren, P. A.; Zucchi, I. A. *Nanotechnology* **2012**, *23*, 115604.
48. Bandara, T. M. W. J.; Dissanayake, M. A. K. L.; Jayasundara, W. J. M. J. S. R.; Albinsson, I.; Mellander, B. E. *Phys. Chem. Chem. Phys* **2012**, *14*, 8620.